doi: 10.34248/bsengineering.1767368



Research Article

Volume 9 - Issue 1: XX-XX / January 2026

A NOVEL WATERMARKING METHOD WITH RESISTANCE TO IMAGE MANIPULATIONS VIA DUAL-TREE COMPLEX WAVELET DOMAIN

Serap ÇAKAR KAMAN^{1*}, Cabir VURAL²

¹Sakarya University, Faculty of Computer and Information Science, Department of Computer Engineering, 54187, Sakarya, Türkiye ²Marmara University, Electrical and Electronics Engineering, 34722, İstanbul, Türkiye

Abstract: A new digital image watermarking method based on dual-tree complex wavelet transform is proposed. The proposed method is shown to be robust to geometric and non-geometric modifications performed on the watermarked image. The complex wavelet domain for watermark insertion gives rise to robustness for non-geometric modifications, while the image normalization provides robustness against geometric modifications. First, the original image is normalized. Then, a watermark is generated such that the capacity is more than one bit according to the properties of the human visual system, and it is added to the three detail subbands coefficients of the normalized image at the first decomposition level in the complex wavelet domain. Finally, successive applications of the inverse complex wavelet transform and the inverse normalization give the watermarked image. Computer simulations show that the method is robust to numerous image manipulations and is superior to the existing digital image watermarking approaches. However, the implementation of the complex wavelet transform is computationally costly. Hence, dual tree implementation is used to reduce computational complexity in the experiments.

Keywords: Digital image watermarking, Image normalization, DT-CWT

*Corresponding author: Sakarya University, Faculty of Computer and Information Science, Department of Computer Engineering, 54187, Sakarya, Türkiye.

E mail: scakar@sakarya.edu.tr (S. ÇAKAR KAMAN) Serap ÇAKAR KAMAN

Cabir VURAL



https://orcid.org/0000-0002-3682-0831 https://orcid.org/0000-0002-9683-3861

Received: August 17, 2025 Accepted: November 15, 2025 Published: January 15, 2026

Cite as: Çakar Kaman, S., & Vural, C. (2026). A novel watermarking method with resistance to image manipulations via dual-tree complex wavelet domain. Black Sea Journal of Engineering and Science, 9(1), xx-xx.

1. Introduction

The need to protect digital data, such as audio, image, and video, against unlawful purposes has become crucial during the last two decades, since the distribution and copying of digital data is easy. Digital watermarking, which is the process of inserting an information-bearing digital signal into the digital data that we wish to protect, has been proposed to solve this important problem. The original data, added signal, and modified signal are called the host signal, watermark, and watermarked signal, respectively. Digital watermarking plays a key role in multiple domains, including intellectual property fingerprinting, anti-piracy protection, broadcast surveillance, data verification, indexing, and covert data embedding. Requirements for a digital watermarking algorithm change for a given application. Transparency, capacity, robustness modifications, security, and whether the original data is required or not to decode the watermark are the most common requirements. It is well known that all the requirements cannot be satisfied simultaneously. The reader is referred to comprehensive tutorials and surveys for more information about the subject (Begum et al., 2020; Kumar et al., 2023; Eldaoushy et al., 2023; Pavan et al., 2023; Dash et al., 2025; Reza et al., 2025). In this study, the focus is on robustness and transparency for digital image watermarking.

A watermarked image may be modified by various intentional or unintentional digital image processing operations. A modification carried out on a watermarked image will be called an attack from now on. The most common attacks are noise addition, filtering, noise removal, compression, taking a statistical average, geometrical attacks (rotation, scaling, translation, etc.), and cropping. Geometrical attacks deserve special attention among these, since even a small geometrical transformation on the watermarked image leads to a loss of synchronization between the watermark encoder and decoder. Several methods have been advanced to combat geometrical attacks, such as Fourier transform and Log Polar Mapping (LPM) (O'Ruanaidh et al., 1998), LPM and phase correlation (Zheng et al., 2003), Zernike moments (Kim et al. 2003), and feature-based methods (Wang et 2008), though the Moment Based Image Normalization (MBIN) was shown to provide the best performance (Dong et al., 2002; Alghoniemy et al., 2004). Many studies have shown that watermarking algorithms designed in the frequency domain have better



performance compared to those designed in the spatial domain for non-geometrical attacks. Among the frequency transformations, the Two-Dimensional (2D) Discrete Wavelet Transform (DWT) is better than other transformations, including the 2D Discrete Cosine Transform and Discrete Fourier Transform, since the 2D DWT has a striking similarity to the Human Visual System (HVS). Although 2D DWT-based methods consider the characteristics of the HVS and perform well in image compression (e.g., JPEG, JPEG 2000), cropping, and median filtering (Barni et. al., 2001), they lack robustness against geometric distortions such as scaling, rotation, and translation.

In recent years, deep learning-based watermarking methods have also been developed. Among these, the MBRS method (Jia et al., 2021), which has an encoder-decoder structure and uses a deep neural network (DNN) for data embedding and extraction; the HiDDeN method (Zhu et al., 2018), based on a convolutional neural network (CNN) with an end-to-end encoder-decoder-adversary architecture; and the RivaGAN method (Zhang et al., 2019), which combines CNN and attention mechanisms for invisible watermarking on video, stand out. While these methods are highly robust to image compression, they lack sufficient robustness to geometric transformations and filtering operations, and have a very high computational cost.

In our previous study, a digital image watermarking algorithm was built by combining the strengths of the MBIN and the 2D DWT (Kazan, 2009). Effects of image normalization on watermarking performed in the 2D DWT domain were investigated for many types of geometrical and non-geometrical attacks. Better bit error rates were obtained, especially for geometrical attacks, when normalization is used. The main shortcoming of the 2D DWT is its dependence on translation. In other words, small translations in an image may cause severe changes between energy distributions of the 2D DWT coefficients at different scales. Another important limitation of the 2D DWT is its poor selectivity for diagonal features. 2D DWT decomposes an image along the horizontal (0°), vertical (90°), and diagonal (±45°) directions. For this reason, 2D DWT cannot distinguish opposite diagonal (±45°) directions. Recently, the 2D Complex Wavelet Transform (CWT) has been developed to deal with the limitations of the 2D DWT (Lawton, 1993). 2D CWT coefficients of an image are not affected if the image is shifted. Furthermore, 2D CWT decomposes an image along the ±150, ±750, and ±450 directions, and it can distinguish opposite diagonal directions. In addition to these two advantages, 2D CWT has also the following properties: (i) it allows for perfect reconstruction by using short filters with linear phase, (ii) it has a redundancy of 4 for finite 2D signals (redundancy of 2d for d-dimensional signals, note that DWT has always redundancy of 1 irrespective of dimension) (iii) it has the lowest computational load the shift-invariant transformations. among

interested reader can find details about 2D CWT in (Selesnick et al., 2005).

Owing to the superiority of the CWT over the DWT, watermarking in the CWT domain is expected to excel over watermarking in the DWT domain. Loo and Kingsbury used this idea and developed the first digital image watermarking algorithm based on the CWT (Loo et al., 2000). After their seminal work, a number of CWTbased digital image processing algorithms have been proposed (Liu et al., 2010; Guo et al., 2010; Yang et al., 2010). Encouraged by the results of the studies, we derive a new image watermarking algorithm based on the MBIN and the 2D CWT in this study. The complex wavelet domain for watermark insertion gives rise to robustness for non-geometric modifications, while the image normalization provides robustness against geometric modifications. First, the original image is normalized. Then, a watermark is generated such that the payload (equivalently, capacity) is more than one bit according to the properties of the HVS, and it is added to the six detail subbands coefficients of the normalized image at the first decomposition level in the 2D CWT domain. Finally, successive inverse applications of the 2D CWT and normalization give the watermarked image. Note that even though both this study and our previous work (Kazan, 2009) use image normalization, they are quite distinct from each other because watermark generation, HVS modelling, watermark insertion, and decoding are completely different in each case. Computer simulations show that the method is robust to numerous image manipulations and is superior to the existing digital image watermarking approaches. However, implementation of the 2D CWT is computationally prohibitive. Recently, a Dual Tree (DT) implementation of the 2D CWT called 2D DT-CWT was developed to reduce computational complexity significantly (Kazan, 2009). For this reason, 2D DT-CWT implementation was preferred in this study.

The study consists of the following. Background information is given in Section 2. Section 3 discusses the proposed method. Section 4 is devoted to determining the robustness of the suggested approach against several attacks and comparing it to two existing algorithms by means of computer simulations. Finally, Section 5 summarizes the study by highlighting the most important observations and listing some possible future research directions.

2. Materials and Methods

2.1. Moment Base Image Normalization

Note that any geometric modification can be represented as an affine transform. Therefore, the goal in image normalization is to apply a transformation to a digital image such that the image and its affine transforms are as similar as possible. The significance of such a transformation is clear. Synchronization between the watermark encoder and decoder is not lost because of a geometric modification applied to the watermarked

image if normalization is performed prior to watermark encoding and decoding. This claim can be justified as follows. Suppose that a watermark is added to a digital image after the image is normalized. Then, inverse normalization is applied to form the watermarked image. The inserted message (or watermark) can be decoded reliably even if the watermarked image undergoes a geometric modification if decoding is carried out after the modified watermarked image is normalized. This is because the original and modified watermarked images have the same normalized image.

The concept of image normalization using geometric moments was originally developed for pattern recognition problems (Wood, 1996; Shen et al., 1997; Rothe et al., 1996). Geometric moments were used to provide invariance for geometric distortions for digital image watermarking in (Wang et al., 2008, and Alghoniemy et al., 2004). Invariant watermark and MBIN are two possible approaches to achieve image normalization (Alghoniemy et al., 2004). An invariant watermark is generated based on moment invariants computed from the image to be watermarked. In MBIN, geometric moments are used as parameters in the normalization process. We have chosen to use the MBIN approach in this study, though it would be interesting to implement the invariant watermark approach in future research to see whether results are affected much.

The following discussion assumes that a general affine transformation can be decomposed into several components. Even though several decompositions exist, we have chosen the one described in (Dong et al., 2002) since it has good stability properties. Any affine matrix is shown to be equivalent to successive applications of translation, shearing, and scaling in both horizontal and vertical directions in (Dong et al., 2002). Therefore, normalization consists of four steps designed so that the effects of these distortions are eliminated.

Geometric moments m_{pq} and central moments μ_{pq} defined below, are used to form the normalized image (equations 1 and 2).

$$m_{pq} = \sum_{x=0}^{M-1} \sum_{y=0}^{N-1} x^p y^p f(x, y)$$
 (1)

$$\mu_{pq} = \sum_{x=0}^{M-1} \sum_{y=0}^{N-1} (x - \bar{x})^p (y - \bar{y})^p f(x, y)$$
 (2)

where p,q=0,1..., $\bar{x}=m_{10}/m_{00}$, $\bar{y}=m_{01}/m_{00}$, and MxN is the size of the image to be watermarked. Applying the following three Spatial Coordinate Transformations (SCTs) successively to the host image f(x,y) results in the normalized image.

Translational invariance is achieved by shifting f(x, y) to its central point. Let $f_c(x_c, y_c)$ denote the centralized image obtained by using the SCT given by equation 3.

$$x_c = x - \bar{x}, \quad y_c = y - \bar{y} \tag{3}$$

Spatial coordinates of the scaled image $f_s(x_s, y_s)$ determined from the spatial coordinates of $f_c(x_c, y_c)$ will be denoted by (x_s, y_s) . Using the SCT given in equation 4 provides invariance to scaling.

$$\begin{pmatrix} x_s \\ y_s \end{pmatrix} = \begin{pmatrix} \alpha & 0 \\ 0 & \delta \end{pmatrix} \begin{pmatrix} x_c \\ y_c \end{pmatrix} \tag{4}$$

where α and δ are computed from equation 5.

$$\alpha = \mp \frac{1}{\sqrt{\mu_{20}^{(c)}}}, \qquad \delta = \mp \frac{1}{\sqrt{\mu_{02}^{(c)}}}$$
 (5)

Among the possible solutions, $\mu_{50}^{(s)} > 0$ and $\mu_{05}^{(s)} > 0$ is chosen. Finally, let (x_n, y_n) denote the spatial coordinates of $f_n(x_n, y_n)$ determined from those of $f_s(x_s, y_s)$. The following SCT gives rise to rotation invariance (equation 6).

$$\binom{x_n}{y_n} = \binom{\cos(\phi) & \sin(\phi)}{-\sin(\phi)} \binom{x_s}{y_s}$$
 (6)

where the rotation angle is computed from equation 7.

$$\phi_1 = tan^{-1} \left(-\frac{\mu_{30}^{(s)} + \mu_{12}^{(s)}}{\mu_{03}^{(s)} + \mu_{21}^{(s)}} \right), \ \phi_2 = \phi_1 + \pi$$
 (7)

Among the two possible solutions, the one for which $\mu_{03}^{(n)} + \mu_{21}^{(n)}$ is taken.

In short, successive applications of the above three SCTs given in equations 3, 4, and 6 to the host image f(x, y) form the normalized image $f_n(x_n, y_n)$. Note that in SCT equations, superscripts indicate the image from which moments are calculated. Figure 1 illustrates that the above procedure indeed provides geometric invariance. The cameraman shown in Figure 1(a) was subjected to several geometric attacks to obtain the distorted image shown in Figure 1(b). Then, both images were normalized. As can be seen from Figure 1(c), the distorted and the original images have the same normalized image.

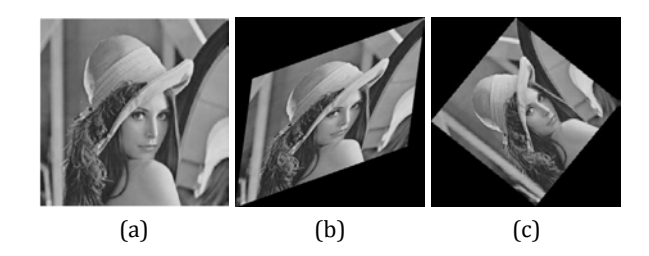


Figure 1. Effect of the moment-based image normalization. (a) Original, (b) distorted, and (c) normalized image obtained from both (a) and (b).

2.2. Dual Tree Complex Wavelet Transform

Wavelet-based techniques are widely used in signal and image processing, but the traditional discrete wavelet transform (DWT) has key limitations. It is extremely sensitive to small shifts in the input signal and lacks directional selectivity. Even a slight displacement in an

impulse signal can lead to major changes in the DWT coefficients' energy distribution. Furthermore, the 2D DWT decomposes images only into horizontal, vertical, and diagonal components (0°, 90°, and $\pm 45^{\circ}$), making it unable to clearly distinguish between $\pm 45^{\circ}$ and $\pm 45^{\circ}$ orientations. This causes ambiguity in the spatial domain, notably in the HH subband, where a checkerboard artifact appears due to mixed diagonal responses (Selesnick et al., 2005).

Complex wavelets can be used to overcome this. A complex wavelet with frequency support limited to one side results in 2D wavelets that are oriented in a specific direction. Taking the real part of such complex wavelets produces real wavelets with directional selectivity and without the checkerboard effect. By constructing several of these wavelets, it is possible to isolate features at directions such as $\pm 15^{\circ}$, $\pm 45^{\circ}$, and $\pm 75^{\circ}$, achieving finer angular resolution than standard DWT.

However, designing complex filters that maintain perfect reconstruction (PR) is difficult and can amplify noise. To address this challenge, the DT-CWT was introduced. It avoids the need for complex-valued filters by using two parallel filter banks with real coefficients—each forming a standard DWT. The filters in these two banks are designed so that one is Hilbert transform of the other. This setup creates approximately analytic wavelets, enabling directional selectivity and improved shift invariance.

Figure 2 illustrates the analysis and synthesis structure of DT-CWT. In the analysis section, two filter banks (FB) are used: the upper tree with filters H_{0a} and H_{1a} , and the lower tree with filters H_{0b} and H_{1b} . These filters are carefully designed to meet the PR condition and to form a Hilbert transform pair. In synthesis, matching filters are used to PR the original signal. This structure enables the DT-CWT to produce complex wavelet coefficients from real filters, achieving the benefits of complex wavelet analysis without direct complex filter design.

In 2D DT-CWT, this dual-tree structure is applied separately to the rows and columns of the image. As a result, instead of three subbands like in 2D DWT, DT-CWT produces six directional subbands at each level of decomposition, corresponding to ±15°, ±45°, and ±75°. These subbands enhance the transform's ability to analyze textures and edges in specific orientations.

Figure 3 shows an example of applying 2D DT-CWT to the Lena image. The decomposition results reveal six oriented subbands, each capturing directional information more effectively than standard DWT. The clearer separation of edge and texture details in different directions highlights the practical advantage of DT-CWT in image analysis.

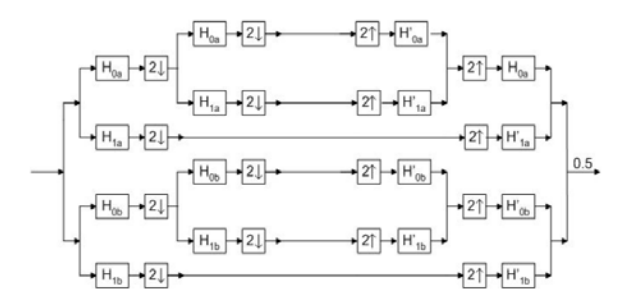


Figure 2. Dual-tree discrete CWT analysis and synthesis filter banks.

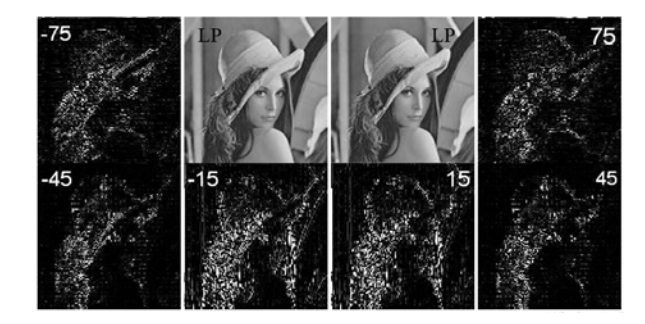


Figure 3. Dual tree complex wavelet coefficients images.

2.3. Watermarking Algorithm

As stated in Part 2.2, when the DT-CWT of an image is calculated, there are six lower bands at each level. Therefore, we have to find the level of 2D DT-CWT to be calculated for watermarking purposes and the lower bands to which the watermark should be included. After the simulations were conducted, it was determined that the best result was obtained for perceptual transparency and strength when six lower bands were used at the first level for applying the watermark. The watermark insertion and detection details are provided in the following subsections.

2.3.1. Watermark insertion

Figure 4 illustrates the watermark embedding method, and the process can be outlined in the following steps. The cover image is assumed to have dimensions of 2Mx2N, and the watermark signal is considered to contain P bits:

- In order to obtain the normalized image $f_n(x_n,y_n)$, the watermark will be included by using the transaction under Part 2.1, and the image of f(x,y) will be normalized.
- Single-level 2D DT-CWT $I_0^{\theta}(i,j)$, of $f_n(x_n,y_n)$ will be calculated.
- Assuming k=1,...,P for $\theta=0,1,....5$, it is ± 1 , otherwise six units of two-dimensional supposed-random $X_0,k^\theta(i,j)$ marks are produced, which have no statistical relationship in $M \times N$ dimensions, formed by zero values (the θ value indicates the lower bands in 2D DT-CWT of $f_n(x_n,y_n)$).

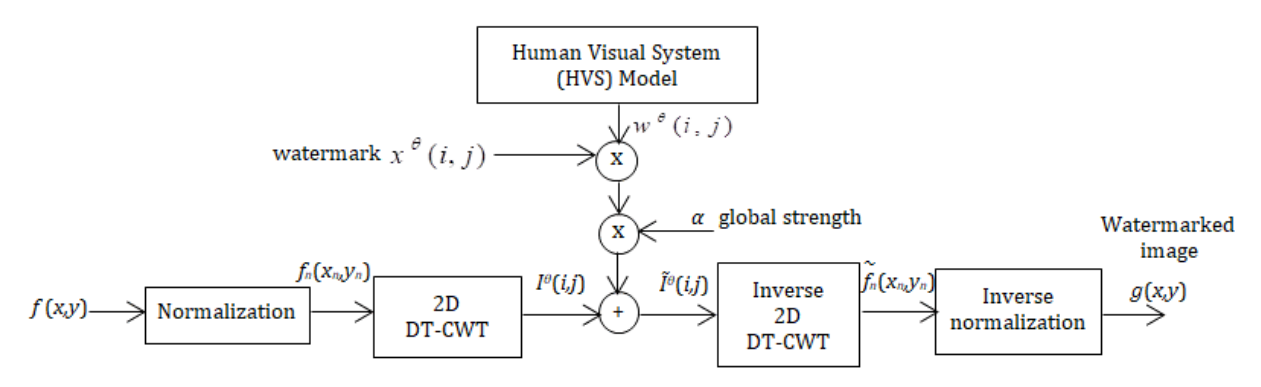


Figure 4. Block diagram of the proposed method.

- lst bit in the m_l watermark (0 or 1), the equation 8.

$$X_0^{\theta}(i,j) = \sum_{k=0}^{P} (2m_k - 1) X_{0,k}^{\theta}(i,j)$$
 (8)

is used, and two dimensioned watermark $X_0\theta(i,j)$ is established.

- The $W_0\theta(i,j)$ masking coefficients, allowing to increase the watermark energy at the locations that the human eye may not perceive, will be determined by using Equation (9) as explained hereinafter.
- As α is a coefficient determining the global energy of the watermark, the watermark is multiplied by $X_0\theta(i,j)$ $\alpha W_0\theta(i,j)$, and the product is added to $I_0\theta(i,j)$ to establish the 2D DT-CWT coefficients as determined with $\tilde{I}_0\theta(i,j)$ for the normalized image.
- The reverse 2D DT-CWT is calculated for $\tilde{I}_{\theta}(ij)$ in order to obtain the normalized watermarked image $\tilde{f}_{n}(x_{n},v_{n})$.
- Reverse normalizing is applied to $\tilde{f}_n(x_n,y_n)$ to establish the watermarked image g(x,y).

The perceptual weight coefficients $w^{\theta}(i,j)$ used in the DT-CWT method are calculated by using human visual perception. The weight constants will be calculated by using equation 9.

$$w^{\theta}(i,j) = \sqrt{k^2 \cdot |I^{\theta}(i,j)|^2 + \gamma^2}$$
(9)

 $\left|I^{\theta}(i,j)\right|^2$ indicates the average square magnitude of transform coefficients in a 3x3 neighborhood whose center is at (i,j), k and γ indicate coefficients that are valued according to each subband. The values for k and γ are given in Table 1.

Table 1. Values of k and γ

Subband	±15°	±75°	±45°
k	1.8	1.8	1.35
γ	2.4	2.4	4

2.3.2. Watermark detection

Let us assume that an attack was applied to the watermarked image g(x,y). As a result of the attack, the watermark detector will take $\tilde{g}(x,y)$ instead of g(x,y). The

watermark detector is a correlation-based detector. Since we have added the watermark in the normalized wavelet space, the correlations should be calculated in the same space. Based on this observation, the kth bit of the watermark will be determined by applying the following steps (Figure 5).

- $\tilde{g}_n(x_{n_n}y_n)$ is obtained applying normalization to $\tilde{g}(x,y)$.
- Single level 2D DT-CWT of the $\tilde{g}_n(x_n,y_n)$ is calculated shown as $\hat{I}_0^{\theta}(i,j)$.
- The correlation ρ_k between k^{th} watermark signal $X_{0,k}\theta(i,j)$ and $\hat{I}_0^{\theta}(i,j)$ is computed from equation 10.

$$\rho_k = \sum_{\theta=0}^{5} \sum_{i=0}^{M-1} \sum_{j=0}^{N-1} \hat{I}_0^{\theta}(i,j) X_{0,k}^{\theta}(i,j)$$
 (10)

The k^{th} bit in the watermark l is decoded as equation 11.

$$\widehat{m}_k = \begin{cases} 1, & \rho_k > 0 \\ 0, & \text{otherwise} \end{cases} \tag{11}$$

All of the bits on the watermark may be determined for k=1,2,...,P by repeating the steps shown in Figure 5. To obtain the optimum watermark detector statistically, the correlation value calculated for each bit may be compared with a threshold value instead of zero. It may be indicated that the optimum threshold value equals zero for the method suggested because of the establishment rule of the watermark signal stated in Section 2.

3. Results and Discussion

Ten images with high, low, mid, and rapid changes were used in the simulations. A 64-bit watermark was embedded into a set of ten 512x512 images, including Baboon, Boats, Bridge, Cameraman, Couple, Elaine, Airplane, Goldhill, Lena, and Peppers. To measure the difference between the watermarked and the original image, the Peak Signal-to-Noise Ratio (PSNR) is used. For the situation in which PSNR is bigger than 35 dB, the image quality is at an acceptable level. Therefore, when the watermark is added to the images, it is noted that the value of PSNR is greater than 35 dB.

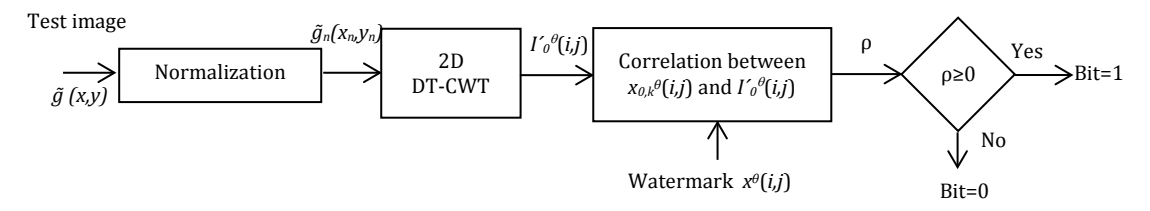


Figure 5. The block diagram of the watermark detector.

To show that the watermark added provides the transparency requirement, the original image in Figure 6 (a), the watermarked image in Figure 6(b), and the difference between them in Figure 6(c) are shown. It is clear from Figure 6(c) that the watermark is inserted into the high-frequency components of the image as it should be.



Figure 6. The method takes HVS into account when inserting the watermark. (a) original, (b) watermarked, (c) difference images (it is scaled by 8).

To test the success of our method, the attacks in Table 2 were applied. The robustness results for rotating, scaling, and JPEG compression are shown in Figure 7, and the robustness against the other attacks is given in Table 3 as Bit Error Rate (BER), the proportion of erroneously decoded bits to the total number of bits that were embedded. When the BER values are calculated, the average of the values for ten images is taken. The watermarks are added to all of these images so that the PSNR value will be 35 dB. The DWT method gives bad results for the rotating attack in Figure 7a. The DCT method gives successful results at small rotating angles, but the performance worsens at large rotating angles. As for the DT-CWT based method, it was successful even at high rotation angles. Figure 7b indicates that all methods give good results at small scale ratios; however, when the scaling ratio is increased, the performance of all methods worsens. On the other hand, the method DT-CWT is superior to the other methods. Similar results are obtained in the JPEG compression (Figure 7c).

As all methods work very well at small compression values, the success rates decrease at high compression ratios. The DT-CWT method gives the best results at all times. The results in Table 3 indicate that the method DT-CWT is superior to other methods for aspect ratio change, affine transform, flipping, and median filtering attacks, except row-column removal. In addition, for a 512x512 image, embedding a watermark takes about 30-100 ms using the DT-CWT+MBIN method, while for methods using deep learning, this process takes an

average of 150-500 ms. Table 4 shows the comparison of the DT-CWT + MBIN method with the current methods that use deep learning.

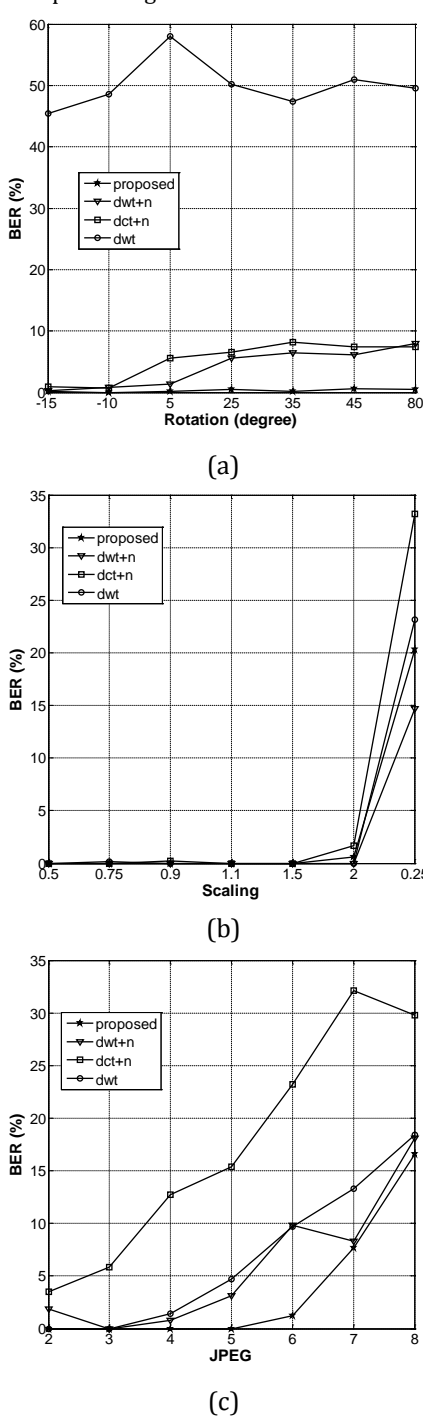


Figure 7. BER curves of the proposed, DWT+N, DCT+N, and DWT methods for (a) rotation, (b) scaling, and (c) JPEG attacks.

Table 2. Attacks used in the experiments to demonstrate the performance of the proposed watermarking method

Attack	Description		
Row-Column Removal	(1,1), (1,5), (5,1), (5,17), (17,5)		
Scaling	0.5, 0.75, 0.9, 1.1, 1.5, 2, 0.25		
Aspect ratio change	(.8,1), (.9,1), (1.1,1), (1.2,1), (1,.8), (1,.9), (1,1.1), (1,1.2)		
Rotation	-15°, -10°, 5°, 25°, 35°, 45°, 80°		
Shearing	(0, %1), (0, %5), (%1, 0), (%5, 0), (%1, %1), (%5, %5)		
Affine transforms	Kernels: $\begin{bmatrix} 1.1 & 0.2 \\ -0.1 & 0.9 \end{bmatrix}$, $\begin{bmatrix} 0.9 & -0.2 \\ 0.1 & 1.2 \end{bmatrix}$, $\begin{bmatrix} -1.01 & -0.2 \\ -0.2 & 0.8 \end{bmatrix}$		
Flipping	Horizontal, vertical		
Median filtering	Kernel sizes: 2x2, 3x3, 4x4		
Filtering	Kernels: $\begin{bmatrix} 0 & -1 & 0 \\ -1 & 5 & -1 \\ 1 & 2 & 1 \end{bmatrix}, \begin{bmatrix} 1 & 2 & 1 \\ 2 & 4 & 2 \\ 1 & 1 & 1 \end{bmatrix}$		
JPEG compression	Quality factors: 2, 3, 4, 5, 6, 7, 8		

Table 3. Decoding performance of the DT-CWT+MBIN (proposed), DWT+MBIN, DCT, and DWT methods in BER for row-column removal, aspect ratio change, shearing, affine transform, flipping, median filtering, and other filtering attacks

Attacks	Method	(a)	(b)	(c)	(d)	(e)	(f)	(g)	(h)
	DT-CWT+MBIN	0	0	0.625	0.781	0.468			
1. Removal	DWT+MBIN	0.156	0	2.031	2.812	2.031			
1. Kelliovai	DCT	2.437	2.046	10.445	4.390	7.906			
	DWT	0	0	0	0	0			
	DT-CWT+MBIN	0	0	0	0	0	0	0	0
2 Aspect ratio	DWT+MBIN	0	0	0	0	0	0	0	0
2. Aspect ratio	DCT	0	0	0	0	0	0	0	0
	DWT	0	0	0	0	0	0	0	0
	DT-CWT+MBIN	0	0	0	0	0	0		
2 Chaorina	DWT+MBIN	0	0	0	0	0	0		
3. Shearing	DCT	0.250	0	1.3438	0.718	0.406	0.406		
	DWT	0	19.531	0	20.937	26.093	35.625		
	DT-CWT+MBIN	0.311	0.155	0.155					
4. Affine	DWT+MBIN	0.937	0.156	0.781					
transforms	DCT	1.968	1.031	1.031					
	DWT	45.937	53.437	52.968					
	DT-CWT+MBIN	0	0						
5. Flipping	DWT+MBIN	0	0						
	DCT	0	0						
	DWT	54.218	50.625						
	DT-CWT+ MBIN	0	0.937	3.125	0	0			
6. Median	DWT+ MBIN	0	0.937	4.531	0	0			
filtering and other filtering	DCT	2.125	7.906	20.875	0	0.562			
outer intering	DWT	0	7.343	40.312	0	0.321			

Table 4. Comparison of DT-CWT + MBIN method with current methods

Criterion / Attack Type	DT-CWT + MBIN	DWT + MBIN	MBRS	HiDDeN	RivaGAN
Geometric attacks (RST, affine, shearing, flip)	Very low BER; native synchronous with MBIN; Successful even in rotation above ±45°	Middle; good at small angles and scales, performance decreases at large angles	Meddle-high; good if differentiable RST is improved with data boosting	Middle; RST attacks require an additional module	Middle; content aware but RST sensitive
JPEG compression	Flawless in high- quality factors; superior to DWT/DCT at low grades, lower than MBRS	Middle	Very high strength (trained with mixed JPEG)	High	High
Filtering (Median, Gaussian)	Low BER	Middle	High	High	High
Computational cost	Middle; Reduced by DT-CWT optimization	Low	High	High	High

4. Conclusions

Most existing digital image watermarking algorithms in the literature treat geometrical and non-geometrical attacks as separate issues. In other words, efficient image algorithms do not exist watermarking simultaneously work for geometric and non-geometric attacks. In this paper, the superiorities of the momentbased image normalizing and 2D DT-CWT are combined, and a new digital image watermarking method has been developed. The method was shown to be robust against rotation, scaling, translation, and IPEG compression. The deficiencies, such as independence of the DWT from the translating and lack of directional selectiveness, are eliminated by using the CWT.

Despite its high robustness against geometric and nongeometric attacks, the proposed method suffers from several limitations. First, the computational complexity of the DT-CWT is higher than that of DCT or DWT, which may be an obstacle for real-time applications or large datasets. Second, the method is designed only for grayscale images, and adapting it to color images requires additional effort. Furthermore, the balance between invisibility and robustness of the watermark depends sensitively on values such as the global power coefficient and HVS parameters, and these parameters may need to be re-optimized for different scenarios. normalization-based synchronization mechanism exhibits limited performance against attacks that involve severe content loss, such as the deletion of a large number of rows or columns.

The studies that may be conducted in subsequent work are listed below:

 When the single tree realization consisting of complex value coefficient filters of the wavelet transform is used, the changes in the results may be tested.

- Other techniques may be used instead of spectrum techniques when establishing a watermark.
- Other HVS methods may be tried instead of the HVS value given in the CWT space.
- The watermark may be included in other lowerband combinations at higher levels instead of six lower bands at the first level.
- Instead of the watermark decomposer based on correlation, an optimum watermark decomposer may be used statistically.
- The required changes may be searched in order to apply the suggested method to the color images and video.
- The superiority of the capacity usage aspect may be seen as an important watermark requirement in addition to the strength of the method.
- The moment stable approach may be applied instead of moment-based image normalizing in order to normalize the image.

Author Contributions

The percentages of the authors' contributions are presented below. All authors reviewed and approved the final version of the manuscript.

	S.Ç.K.	C.V.
С	50	50
D	50	50
S	50	50
L	50	50
W	50	50
CR	50	50
SR	50	50
PM	50	50

C=Concept, D= design, S= supervision, L= literature search, W= writing, CR= critical review, SR= submission and revision, PM= project management.

Conflict of Interest

The authors declared that there is no conflict of interest.

Ethical Consideration

Since no studies involving humans or animals were conducted, ethical committee approval was not required for this study.

References

- Alghoniemy, M., & Tewfik, A. H. (2004). Geometric invariance in image watermarking. *IEEE Transactions on Image Processing*, 13(2), 145–153.
- Barni, M., Bartolini, F., & Piva, A. (2001). Improved wavelet-based watermarking through pixel-wise masking. *IEEE Transactions on Image Processing*, 10(5), 783–791.
- Begum, M., & Uddin, M. S. (2020). Digital image watermarking techniques: A review. *Information*, 11(2), 110.
- Dash, A., Naik, K., & Priyadarshini, P. (2025). Robust digital image watermarking using hybrid optimization technique. In Intelligent Computing Techniques and Applications (pp. 300– 305).
- Dong, P., & Galatsanos, N. P. (2002). Affine transformation resistant watermarking based on image normalization. In *Proceedings of IEEE International Conference on Image Processing* (Vol. 3, pp. 489–492).
- Eldaoushy, A. F., et al. (2023). Efficient hybrid digital image watermarking. *Journal of Optics*, *52*, 2224–2238.
- Guo, L., & Zhou, J. (2010). A new robust digital watermarking based on complex wavelet transform. In *Proceedings of the International Conference on E-Business and E-Government (ICEE)* (pp. 3529–3532).
- Jia, Z., Fang, H., & Zhang, W. (2021). MBRS: Enhancing robustness of DNN-based watermarking by mini-batch of real and simulated JPEG compression. In *Proceedings of the 29th ACM International Conference on Multimedia* (pp. 41–49).
- Kazan, S. (2009). Digital image watermarking methods using moment based normalization (Master's thesis). Institute of Science. Sakarva.
- Kim, H. S., & Lee, H. K. (2003). Invariant image watermark using Zernike moments. *IEEE Transactions on Circuits and Systems for Video Technology*, *13*(8), 766–775.
- Kumar, L., Singh, K. U., & Kumar, I. (2023). A comprehensive review on digital image watermarking techniques. In 2023 International Conference on Computational Intelligence and Sustainable Engineering Solutions (CISES) (pp. 737–743).
- Lawton, W. (1993). Applications of complex valued wavelet transforms to subband decomposition. *IEEE Transactions on Signal Processing*, 41(12), 3566–3568.

- Liu, J., & She, K. (2010). Robust image watermarking using dual tree complex wavelet transform based on human visual system. In *Proceedings of the International Conference on Image Analysis and Signal Processing (IASP)* (pp. 675–679).
- Loo, P., & Kingsbury, N. (2000). Digital watermarking using complex wavelets. *IEEE Transactions on Signal Processing*, 2(3), 29–32.
- O'Ruanaidh, J. J. K., & Pun, T. (1998). Rotation, scale, and translation invariant spread spectrum digital image watermarking. *Signal Processing*, 66(3), 303–317.
- Pavan, A. C., & Somashekara, M. T. (2023). An overview on research trends, challenges, applications and future direction in digital image watermarking. *International Research Journal* on Advanced Science Hub. 5(1).
- Reza, S., Hosen, M. A., Rahman, A., & Galib, S. M. (2025). A hybrid approach to digital image watermarking integrating DWT, DFT, and genetic algorithm. In *International Conference on Artificial Intelligence and Smart Energy* (pp. 484–496).
- Rothe, I., Susse, H., & Voss, K. (1996). The method of normalization to determine invariants. *IEEE Transactions on Pattern Analysis and Machine Intelligence*, *18*(4), 366–376.
- Selesnick, I. W., Baraniuk, R. G., & Kingsbury, N. G. (2005). The dual-tree complex wavelet transform. *IEEE Signal Processing Magazine*, 22(6), 123–151.
- Shen, D., & Ip, H. H. S. (1997). Generalized affine invariant image normalization. *IEEE Transactions on Pattern Analysis and Machine Intelligence*, 19(5), 431–440.
- Wang, X., Hou, L., & Wu, J. (2008). A feature-based robust digital image watermarking against geometric attacks. *Image and Vision Computing*, 26(7), 980–989.
- Wood, J. (1996). Invariant pattern recognition: A review. Pattern Recognition. 29(1), 1–17.
- Yang, H., Jiang, X., & Kot, A. C. (2010). Image watermarking using dual-tree complex wavelet by coefficients swapping and group of coefficients quantization. In *Proceedings of the IEEE International Conference on Multimedia and Expo (ICME)* (pp. 1673–1678).
- Zhang, K. A., Xu, L., Cuesta-Infante, A., & Veeramachaneni, K. (2019). Robust invisible video watermarking with attention. *arXiv*, 1909.01285.
- Zheng, D., Zhao, J., & El Saddik, A. (2003). RST-invariant digital image watermarking based on log-polar mapping and phase correlation. *IEEE Transactions on Circuits and Systems for Video Technology*, 13(8), 753–765.
- Zhu, J., Kaplan, R., Johnson, J., & Fei-Fei, L. (2018). HiDDeN: Hiding data with deep networks. In *Proceedings of the European Conference on Computer Vision (ECCV)* (pp. 657–672).